RSC Advances




ROYAL SOCIETY OF CHEMISTRY

www.rsc.org/advances

# Surface Defects Engineering: Gigantic Enhancement in the Optical and Gas Detection Ability of Metal Oxide Sensor

**Wen-Chieh Wang[a†], Chun-Yen Lai[b†], Yu-Ting Lin[a], Tzu-Hsuan Yua[a], Zong-Yi Chen[a], Wen-Wei Wu[b] and Ping-Hung Yeh[*a]**

[a] Department of Physics, Tamkang University, Tamsui, New Taipei City, 25137, Taiwan

[b] Department of Materials Science and Engineering, National Chiao Tung University, No. 1001, University Road, East District, Hsinchu City 30010, Taiwan

[†]First two authors contribute to this work equally.

*[*] Prof. Ping-Hung Yeh Corresponding-Author,*

*E-mail: ((phyeh331@mail.tku.edu.tw))*

## ABSTRACT

In this work, the detection ability of nanosensors can be improved extraordinary by surface defects engineering. The kinked $SnO_{2-X}$ /$SnO_2$ nanostructure was fabricated by tuning the oxygen flow and used this kinked $SnO_{2-X}$ /$SnO_2$ nanostructure to study the mechanism of surface defect (oxygen vacancy, $V_O$) affection through the electric measurement. For UV light sensing, the response of $SnO_{2-X}$ NW device is always better than $SnO_2$ NW device, two orders higher under pure $O_2$ surrounding condition. The detection mechanism can be clarified by changing the detection environment (oxygen concentration) and the UV light detection sensitivity can be improved by increasing the surface $V_O$ density. Furthermore, the $SnO_{2-X}$ NW device is very sensitive to its surrounding environment due to the high surface $V_O$ density. Hence, the CO/$O_2$ alternate-detection was used to verify our hypothesis; the results show that the $SnO_{2-X}$ NW device presents great detection ability, compared with $SnO_2$ NW device. The sensitivity of $SnO_{2-X}$ NW device is two order enhancements and the reset/response time is faster, compared with $SnO_2$ NW device. To verify this

hypothesis, the polycrystalline structure was fabricated to prove that the detection ability of metal-oxide nanosensors can be improved gigantically by increasing surface defect amount.

Keywords: surface defect, low temperature gas detection, metal-oxide

**Introduction**

Recently, nanomaterials, such as nanowire[1-4], nanobelt[5-7] and nanotube[8-10], polymer material[11], have been extensively studied and utilized to form nano-devices for different application[12-18]. For metal-oxide nanomaterials, because the high surface-to-volume ratio and surface defect of nanostructures, which made the metal-oxide nanomaterials are quite sensitive for the environment variation[19-26]. Many articles reported that Schottky contact mechanism can enhance the performance of metal-oxide nanomaterials, such as piezotronic devices[27, 28], nanogenerators[29-32] and nanosensors[20, 33-39].

For sensor application, using Schottky contact as a control gate can improve the sensitivity, response and reset time[39-42]. Besides, the defect amount of metal-oxide nanomaterials is main parameter for sensor application[43-49]. The surface defect[50] and the oxygen vacancy[51] of meta-oxide nanomaterials have been reported and discussed widely. Many research works tried to control the defect amount and level of metal-oxide in chemical or physical way to create other possibility or application[52-60]. Besides, the signal output of Schottky contact device is strong relative to the surface defect.

Tin dioxide, $SnO_2$, which has potential for ultraviolet (UV) light detection application, due to its large band gap[61]. Otherwise, $SnO_2$ is also a candidate for gas detection because the oxygen vacancy[18, 39, 48, 57, 58]. Besides, $SnO_2$ also can be used as photo-catalyst and solar-cell applications[55, 62-64]. In this research work, the Tin oxide nanomaterials were fabricated with different amounts of defect; and the devices were formed as Schottky gate device for the mechanism investigation. The relativity of the detection ability and defect amount of Tin oxide nanosensor can be figure out by using the Schottky contact devices made with this kinked structure.

**Results and discussion**

The detail analyses of Tin oxide nanostructure (NS) can be obtained from the TEM images, as shown in

Figure 1. The growth direction of Tin oxide NS can be identified from the diffraction pattern and high resolution TEM images, as shown in Figure 1a~c. Due to our synthesis controlling, the oxygen composition of both side would be different; the lower oxygen composition was detected for the NS growth without oxygen flow, as shown in (d)~(f). The schematic and SEM images of nanodevice can be seen in Figure 1 (g). The Pt was deposited by focus ion beam (FIB) to form Ohmic contact; the free contacts of both sides can be formed to be Schottky contacts as detection units[65]. Each side composition of nanodevice can be identified by EDS of SEM system, as illustrated in Figure 1 (h).

For photodetection, the sensitivity of $SnO_{2-X}$ NW device for UV (254nm) light detection is higher than $SnO_2$ NW device; because the dark current ($I_D$) of $SnO_{2-X}$ NW device is smaller than the $I_D$ of $SnO_2$ NW device and the photo current ($I_P$) of $SnO_{2-X}$ NW device is larger than the $I_P$ of $SnO_2$ NW device, respectively, as shown in Figure 2 (a). The temperature of measurement is in room temperature, 25℃. The UV detecting ability of both devices is related to the oxygen concentration of sensing environment, as illustrated in Figure 2 (b). The sensitivity of $SnO_{2-X}$ NW device is always higher than $SnO_2$ NW device, no matter what oxygen concentration percentage is. The UV detection sensitivity of both NW devices will be increased when the oxygen concentration increasing. The sensing mechanism can be illustrated as Figure 2 (c) and (d) for each device.

The $SnO_{2-X}$ NW device has impressive improvement of sensitivity is because that the density of surface oxygen vacancy ($V_O$) is higher. When the UV light off, the $SnO_{2-X}$ NW device would trap more oxygen molecules at Schottky contact interface to form $O_2^-$ and raise the Schottky barrier height (SBH) to reduce the current, so the $I_D$ of $SnO_{2-X}$ NW device would be lower than $SnO_2$ NW device. But when the UV light on, the electron-hole pair would be generated and $O_2^-$ would be desorbed by the hole. Because the hole would combine with the $O_2^-$ to form $O_{2(g)}$ and desorb, that would reduce the SBH to increase the $I_P$. Besides, the lone pair electrons will increase the $I_P$ of $SnO_{2-X}$ NW device, compare with $SnO_2$ NW device, the lone pair electrons amount of $SnO_{2-X}$ NW device is larger, as shown in Figure 2 (c) and (d). Due to above-mentioned

results, the response can be improved no matter what oxygen concentration by using the $SnO_{2-X}$ NW device, compare with $SnO_2$ NW device. The SBH variation also can be analyzed from the electrical measurement, the $\Delta\Phi$ (SBH variation) would be stabled for $SnO_2$ NW device after 40 % oxygen concentration. But for $SnO_{2-X}$ NW device, the $\Delta\Phi$ would be raised with the concentration of oxygen increasing, as shown in Figure 2 (e). The SBH can be approximately presented by the following equation[66]:

$$I_r = AA^{**2} exp[-q\Phi_{eff}/kT]$$

Here, $I_r$ is the reverse bias we set, A is the contact area between $SnO_2$ NW and Pt electrode, $A^{**}$ is the effective Richardson Constant, q is electric charge, $\Phi_{eff}$ is the SBH, k and T is the Boltzmann Constant and system temperature, respectively.

The $\Delta\Phi$ of both devices are almost the same for the oxygen concentration around 20%; but when the oxygen concentration above 40%, the $\Delta\Phi$ would be different. This result symbolizes the surface $V_O$ density of $SnO_{2-X}$ NW device is higher than the $SnO_2$ NW device based on the mechanism illustrated in Figure 2 (c) and (d), which also consists with the TEM and SEM analyses. The SBH differences can be measured and analyzed between $SnO_{2-X}$ and $SnO_2$ NW devices by oxygen concentration variation, and the difference will be enlarged when the oxygen concentration increasing as shown in Table 1 (Detail measurement can be seen in Figure S1). Above result shows that the Tin oxide based NW device would be very sensitive to its surrounding environment, especially for oxygen concentration. So we can presume that Tin oxide based NW device will have great detection ability for gas, especially for $SnO_{2-X}$ NW device.

From our data, the gas detection ability of $SnO_{2-X}$ NW device is better than the $SnO_2$ NW device, as shown in Figure 3. For gas detection, the $O_2$-detection current density (J) was used for base current ($J_0=J_{O_2}$) and the CO-detection current density ($J_{CO}$) was used for reaction current ($J=J_{CO}$). The sensitivity (S) can be defined as $S=\Delta J/J_0$, $\Delta J=J_{CO}- J_{O_2}$. For sensing, the CO detection signal output of $SnO_{2-X}$ NW device is larger than $SnO_2$ NW device, and the $J_0$ of $SnO_{2-X}$ NW device is smaller than $SnO_2$ NW device, can be seen in Figure 3 (a). So that the sensitivity of $SnO_{2-X}$ NW device is higher than $SnO_2$ NW device for each individual

CO concentration detection, as shown in Figure 3 (b). The repetition of both devices can be seen for 2 ppm CO detection can be seen in Figure S3. The detection mechanism can be described in Figure 3 (c). Because the high surface $V_O$ density of $SnO_{2-X}$ NW device, the $J_{O_2}$ can be reduced due to SBH raising since oxygen adsorption. Considering $CO/O_2$ alternate-detection, the SBH variation of $SnO_{2-X}$ NW device is larger than $SnO_2$ NW device. Based on this surface $V_O$ density difference, the improvement of the gas detection abilities (the sensitivity, response and reset time) of $SnO_{2-X}$ NW device are gigantic, compared with $SnO_2$ NW device. From Table 2, we can see higher sensitivity and faster reset time since increasing the CO concentration by using $SnO_{2-X}$ NW device (Detail data can be seen in Figure S2). That is because larger CO concentration can reduce more SBH to have higher current ($J_{CO}$); so when the $O_2$ flow in to raise the SBH, the current ($J_{O_2}$) will be decreased immediately. But the response time is related to the influence of gas-surface interaction, the interaction most depend on the temperature effect. So the response time will be no related with different CO concentration. This results can support our hypothesis, which increasing surface defects can improve the response. So we synthesized another polycrystalline nanostructure to reconfirm our hypothesis. The polycrystalline structure we use is $SnO_2$ (p-$SnO_2$) and ZnO (p-ZnO) nanowire to compare with single-crystalline $SnO_2$ (s- $SnO_2$). The sensitivity enhancements of p-$SnO_2$ and p-ZnO are two order larger than s-$SnO_2$ by the UV light detection; The sensitivities of s-$SnO_2$, p-$SnO_2$ and p-ZnO are 9.4 %, 132.3 % and 130.7 %, as seen in Figure S4.

**Experiment**

Asymmetric kinked $SnO_2$ /$SnO_{2-X}$ nanowires

The kinked $SnO_{2-X}$/$SnO_2$ NWs were synthesized on silicon substrates at 850 $^oC$ via the general catalyst free thermal evaporation method using $SnO_2$ and carbon powders as sources in a horizontal quartz tube connected to vacuum pump and a programmable mass flow controller (MFC). The source was placed in an alumina boated located at the high temperature zone 1000 $^oC$. The substrates then positioned in the source downstream. After the tube had been sealed and evacuated to the base pressure, a carrier gas, $Ar/O_2$, was kept flowing through the tube to direct the deposition process. Initially, $SnO_2$ NWs were grown in 10

standard cubic cemtimeters per minute (s.c.c.m.) $Ar/O_2$ mixture gas with the volume ratio of 5:1 for 15 min to create the stoichiometric $SnO_2$ segment, as shown in Figure S5. After reaction, the oxygen input was turned off, and the background pressure was kept at 4 torr to create the $SnO_{2-X}$ segment. The growth plane of the kinked NW shifts from (200) to (002) owing to the external pressure perturbation.

**Conclusions**

In this research work, we have demonstrated that the kinked $SnO_{2-X}/SnO_2$ nanostructure can be formed by controlling the oxygen flow; used this kinked $SnO_{2-X}/SnO_2$ nanostructure to form Schottky contact devices and to study the affection of the surface $V_O$ density through the optical and gas condition electric measurement. For UV light detection, the gigantic enhancement in sensitivity of $SnO_{2-X}$ NW device is because the $V_O$ can generate more electron-hole pairs to improve the photo response. We also studied the mechanism by controlling the detection environment (oxygen concentration) and we figured out that the $\Delta\Phi$ is related with oxygen concentration. Based on this result, we found that the $SnO_{2-X}$ NW device is quite sensitive to its surrounding environment. So we used the $CO/O_2$ alternate-detection to verify our hypothesis and the results show that the $SnO_{2-X}$ NW device presents great detection ability, compared with $SnO_2$ NW device. The sensitivities of the $SnO_{2-X}$ NW device are two order larger than the $SnO_2$ NW device when CO concentration over 50 ppm. The response and reset time all improved by using the $SnO_{2-X}$ NW device. We proved that increasing the surface defects and using Schottky contact can improve the detection ability of metal-oxide nanosensors extraordinary. Based on above idea, we also designed another nanostructure, polycrystalline nanostructure, to reconfirm the hypothesis. The sensitivities of p-$SnO_2$.and p-ZnO devices are 132.3 % and 130.7 %, all perform better than s-$SnO_2$, 9.4 %. We can use the technology of material science engineering and physics to design high-resolution and fast monitor speed nanosensor.

**Acknowledgements**

This research was supported by the Ministry of Science and Technology, Taiwan, under grants NSC-101-2112-M-032-004-MY3 and MOST-104-2112-M-032-003-006

**Figure captions**

Figure 1. (a) Low magnification TEM image of a kinked $SnO_{2-X}/SnO_2$ nanostructure with the growth orientation changed from (200) to (002), the growth orientation can be indicated by the selected area electron diffraction (SAED) pattern in the inset. (b) and (c) show the high resolution images and lattice constant of $SnO_2$ and $SnO_{2-X}$, respectively. (d) The Sn and O concentrations of a kinked $SnO_{2-X}/SnO_2$ nanowire can be analyzed by EDS element line scan. (e) and (f) show the elemental mapping of Sn and O, respectively. (g) Schematic diagram and SEM image of $SnO_{2-X}/SnO_2$ nanowire Schottky contacted device. (h) EDS analysis and the atomic percent data of $SnO_{2-X}/SnO_2$ NWs.

Figure.2 (a) 254nm UV detection performance in 40% oxygen gas environment (with 40% oxygen and 60% nitrogen). (b) The sensitivities in different oxygen concentration of $SnO_{2-X}$ and $SnO_2$ NW devices. (c) and (d) show the mechanism diagrams of $SnO_{2-X}$ and $SnO_2$ NW devices of oxygen molecules interaction at the interface. Step (i) and (ii) represent the adsorption of oxygen molecules. (iii) shows the desorption of oxygen molecules by UV illumined. The $SnO_{2-X}$ NW device has higher sensitivity is because that the $V_O$ is higher. When the UV light off, more oxygen molecules were trapped at Schottky contact interface to form $O_2^-$ and raise the Schottky batrrier height (SBH) to reduce the current, so the $I_d$ of $SnO_{2-X}$ NW device was lower. But turn on the UV light, the electron-hole pairs would be generated and $O_2^-$ would be desorbed by the hole. Because the hole would combine with the $O_2^-$ to form $O_{2(g)}$ and desorb, that would reduce the SBH to increase the $I_P$. (e) The variation of SBH from vacuum environment to pure oxygen environment (with 100% oxygen) of $SnO_{2-X}$ and $SnO_2$ NW devices.

Figure.3 (a) represents detection performance of $O_2$ with different CO concentration sensing at 200 °C operation temperature. (b) The sensitivities of $SnO_{2-X}$ NW device are higher than $SnO_2$ NW device for different CO concentrations detection. (c) shows the detection mechanism of $SnO_{2-X}$ and $SnO_2$ NW devices. Considering $CO/O_2$ alternate-detection, the SBH variation of $SnO_{2-X}$ NW device is larger than $SnO_2$ NW device ($\Delta\Phi_{SnO_{2-X}} > \Delta\Phi_{SnO_2}$), that is due to the high surface $V_O$ density of $SnO_{2-X}$ NW device.

**Table 1. The variation and difference of two schottky barrier height in different $O_2$ concentration environment.**

| Oxygen concentration (y%) | $\Delta\Phi_{y\% - y\text{-}20\%}$ | | $\Phi_{SnO_{2-X}} - \Phi_{SnO_2}$ |
|---|---|---|---|
| | $SnO_{2-X}$ | $SnO_2$ | |
| 0% | - | - | - |
| 20% | 85 meV | 83 meV | 2 meV |
| 40% | 27 meV | 21 meV | 8 meV |
| 60% | 6 meV | 3 meV | 11 meV |
| 80% | 18 meV | 5 meV | 25 meV |
| 100% | 26 meV | 4 meV | 47 meV |

**Table 2. The sensitivity, response time and reset time of different CO concentration gas sensing.**

| CO concentration | | Sensitivity | $\tau_{response}$ | $\tau_{reset}$ |
|---|---|---|---|---|
| 2 ppm | $SnO_{2-X}$ | 490 % ± 43 % | 169 s | 221 s |
| | $SnO_2$ | 75 % ± 7 % | 180 s | 238 s |
| 50 ppm | $SnO_{2-X}$ | 27549 % ± 1521 % | 234 s | 7 s |
| | $SnO_2$ | 254 % ± 53 % | 451 s | 9 s |
| 100 ppm | $SnO_{2-X}$ | 43657 % ± 2232 % | 420 s | 2 s |
| | $SnO_2$ | 541 % ± 124 % | 630 s | 3 s |
| 200 ppm | $SnO_{2-X}$ | 46726 % ± 780 % | 225 s | <1 s |
| | $SnO_2$ | 551 % ± 76 % | 341 s | 2 s |

## References


1. S. Xu and Z. Wang, *Nano Res.*, 2011, **4**, 1013-1098.
2. P. Gao and Z. Wang, in *Scanning Microscopy for Nanotechnology*, Springer New York, 2007, ch. 13, pp. 384-426.
3. Ü. Özgür, Y. I. Alivov, C. Liu, A. Teke, M. A. Reshchikov, S. Doğan, V. Avrutin, S. J. Cho and H. Morkoç, *J. Appl. Phys.*, 2005, **98**, 041301.
4. Z. Wang, *Chinese Sci. Bull.*, 2009, **54**, 4021-4034.
5. J. Wang, D. N. Tafen, J. P. Lewis, Z. Hong, A. Manivannan, M. Zhi, M. Li and N. Wu, *J. Am. Chem. Soc.*, 2009, **131**, 12290-12297.
6. K. Shankar, J. I. Basham, N. K. Allam, O. K. Varghese, G. K. Mor, X. Feng, M. Paulose, J. A. Seabold, K.-S. Choi and C. A. Grimes, *J. Phys. Chem. C*, 2009, **113**, 6327-6359.
7. O. Lupan, T. Braniste, M. Deng, L. Ghimpu, I. Paulowicz, Y. K. Mishra, L. Kienle, R. Adelung and I. Tiginyanu, *Sensor. Actuat. B-Chem.*, 2015, **221**, 544-555.
8. G. She, X. Huang, L. Jin, X. Qi, L. Mu and W. Shi, *Small*, 2014, **10**, 4685-4692.
9. S. Y. Yang, W. Choi and H. Park, *ACS Appl. Mater. Interfaces*, 2015, **7**, 1907-1914.
10. D. H. Kim, Y.-S. Shim, J.-M. Jeon, H. Y. Jeong, S. S. Park, Y.-W. Kim, J.-S. Kim, J.-H. Lee and H. W. Jang, *ACS Appl. Mater. Interfaces*, 2014, **6**, 14779-14784.
11. Y. Gao, Y. Zhao, L. Qiu, Z. Guo, D. O'Hare and Q. Wang, *Polymer Composites*, 2015, DOI: 10.1002/pc.23764.
12. X. Wang, N. Aroonyadet, Y. Zhang, M. Mecklenburg, X. Fang, H. Chen, E. Goo and C. Zhou, *Nano Lett.*, 2014, **14**, 3014-3022.
13. L. Peng, L. Hu and X. Fang, *Adv. Funct. Mater.*, 2014, **24**, 2591-2610.
14. S. Jeong, M. Choe, J.-W. Kang, M. W. Kim, W. G. Jung, Y.-C. Leem, J. Chun, B.-J. Kim and S.-J. Park, *ACS Appl. Mater. Interfaces*, 2014, **6**, 6170-6176.
15. A. Pescaglini, A. Martín, D. Cammi, G. Juska, C. Ronning, E. Pelucchi and D. Iacopino, *Nano Lett.*, 2014, **14**, 6202-6209.
16. X. Yang, R. Liu, C. Du, P. Dai, Z. Zheng and D. Wang, *ACS Appl. Mater. Interfaces*, 2014, **6**, 12005-12011.
17. N. A. Kyeremateng, *ChemElectroChem*, 2014, **1**, 1442-1466.
18. M. Law, H. Kind, B. Messer, F. Kim and P. Yang, *Angewandte Chemie*, 2002, **114**, 2511-2514.
19. G. F. Fine, L. M. Cavanagh, A. Afonja and R. Binions, *Sensors*, 2010, **10**.
20. Z. Yang, X. Dou, S. Zhang, L. Guo, B. Zu, Z. Wu and H. Zeng, *Adv. Funct. Mater.*, 2015, **25**, 4039-4048.
21. H. S. Woo, C. H. Kwak, J. H. Chung and J. H. Lee, *ACS Appl. Mater. Interfaces*, 2014, **6**, 22553-22560.
22. S. W. Choi, A. Katoch, G. J. Sun, J. H. Kim, S. H. Kim and S. S. Kim, *ACS Appl. Mater. Interfaces*, 2014, **6**, 8281-8287.
23. A. Katoch, J. H. Kim and S. S. Kim, *ACS Appl. Mater. Interfaces*, 2014, **6**, 21494-21499.
24. H. Zhou, R. Deng, Y.-F. Li, B. Yao, Z.-H. Ding, Q.-X. Wang, Y. Han, T. Wu and L. Liu, *J. Phys. Chem. C*, 2014, **118**, 6365-6371.
25. F. Hernández-Ramírez, J. Rodríguez, O. Casals, E. Russinyol, A. Vilà, A. Romano-Rodríguez, J. R. Morante and M. Abid, *Sensor. Actuat. B-Chem.*, 2006, **118**, 198-203.
26. F. Hernández-Ramírez, A. Tarancón, O. Casals, J. Arbiol, A. Romano-Rodríguez and J. R. Morante, *Sensor. Actuat. B-Chem.*, 2007, **121**, 3-17.
27. Z. L. Wang, in *Piezotronics and Piezo-Phototronics*, Springer Berlin Heidelberg, 2012, ch. 1, pp. 1-17.
28. R. Yu, C. Pan, J. Chen, G. Zhu and Z. L. Wang, *Adv. Funct. Mater.*, 2013, **23**, 5868-5874.
29. W. Seung, M. K. Gupta, K. Y. Lee, K.-S. Shin, J.-H. Lee, T. Y. Kim, S. Kim, J. Lin, J. H. Kim and S.-W. Kim,

*ACS Nano*, 2015, **9**, 3501-3509.
30. L. W. Yamin, in *Piezoelectric ZnO Nanostructure for Energy Harvesting*, John Wiley & Sons, Inc., 2015, ch. 4, pp. 65-103.
31. S. Garain, T. K. Sinha, P. Adhikary, K. Henkel, S. Sen, S. Ram, C. Sinha, D. Schmeißer and D. Mandal, *ACS Appl. Mater. Interfaces*, 2015, **7**, 1298-1307.
32. Y. Wu, Q. Jing, J. Chen, P. Bai, J. Bai, G. Zhu, Y. Su and Z. L. Wang, *Adv. Funct. Mater.*, 2015, **25**, 2166-2174.
33. T.-Y. Wei, P.-H. Yeh, S.-Y. Lu and Z. L. Wang, *J. Am. Chem. Soc.*, 2009, **131**, 17690-17695.
34. C. Pan, R. Yu, S. Niu, G. Zhu and Z. L. Wang, *ACS Nano*, 2013, **7**, 1803-1810.
35. Y. Hu, J. Zhou, P. H. Yeh, Z. Li, T. Y. Wei and Z. L. Wang, *Adv. Mater*, 2010, **22**, 3327-3332.
36. P. Chinnamuthu, J. C. Dhar, A. Mondal, A. Bhattacharyya and N. K. Singh, *J. Phys. D: Appl. Phys.*, 2012, **45**, 135102.
37. S. Lenaerts, J. Roggen and G. Maes, *Spectrochimica Acta Part A: Molecular and Biomolecular Spectroscopy*, 1995, **51**, 883-894.
38. E. R. Viana, J. C. González, G. M. Ribeiro and A. G. de Oliveira, *J. Phys. Chem. C*, 2013, **117**, 7844-7849.
39. C.-M. Chang, C.-H. Hsu, Y.-W. Liu, T.-C. Chien, C.-H. Sung and P.-H. Yeh, *Nanoscale*, 2015, **7**, 20126-20131.
40. Y.-H. Zhang, L.-F. Han, Y.-H. Xiao, D.-Z. Jia, Z.-H. Guo and F. Li, *Computational Materials Science*, 2013, **69**, 222-228.
41. C.-H. Sung, T.-C. Chien, C.-M. Chang, C.-M. Chang and P.-H. Yeh, *RSC Adv.*, 2015, **5**, 16769-16773.
42. J. K. Hsu, T. Y. Lin, C. Y. Lai, T. C. Chien, J. H. Song and P. H. Yeh, *Appl. Phys. Lett.*, 2013, **103**, 123507.
43. N. O. Savage, S. A. Akbar and P. K. Dutta, *Sensor. Actuat. B-Chem.*, 2001, **72**, 239-248.
44. C. S. Moon, H.-R. Kim, G. Auchterlonie, J. Drennan and J.-H. Lee, *Sensor. Actuat. B-Chem.*, 2008, **131**, 556-564.
45. Q. H. Li, T. Gao, Y. G. Wang and T. H. Wang, *Appl. Phys. Lett.*, 2005, **86**, 123117.
46. S. Mathur, S. Barth, H. Shen, J.-C. Pyun and U. Werner, *Small*, 2005, **1**, 713-717.
47. M. K. Nowotny, L. R. Sheppard, T. Bak and J. Nowotny, *J. Phys. Chem. C*, 2008, **112**, 5275-5300.
48. S. Das and V. Jayaraman, *Progress in Materials Science*, 2014, **66**, 112-255.
49. J. Nisar, Z. Topalian, A. De Sarkar, L. Österlund and R. Ahuja, *ACS Appl. Mater. Interfaces*, 2013, **5**, 8516-8522.
50. G. Pacchioni, *Physical Chemistry Chemical Physics*, 2013, **15**, 1737-1757.
51. X. Pan, M.-Q. Yang, X. Fu, N. Zhang and Y.-J. Xu, *Nanoscale*, 2013, **5**, 3601-3614.
52. C. Shoou-Jinn, H. Ting-Jen, I. C. Chen and H. Bohr-Ran, *Nanotechnology*, 2008, **19**, 175502.
53. J. M. Wu, Y.-R. Chen and W. T. Kao, *ACS Appl. Mater. Interfaces*, 2014, **6**, 487-494.
54. A. Kar, S. Kundu and A. Patra, *J. Phys. Chem. C*, 2010, **115**, 118-124.
55. Y. Zhang, A. Kolmakov, S. Chretien, H. Metiu and M. Moskovits, *Nano Lett.*, 2004, **4**, 403-407.
56. S. Bhaumik, A. K. Sinha, S. K. Ray and A. K. Das, *IEEE Trans. Magn.*, 2014, **50**, 1-6.
57. J. Pan, R. Ganesan, H. Shen and S. Mathur, *J. Phys. Chem. C*, 2010, **114**, 8245-8250.
58. F. Hernandez-Ramirez, J. D. Prades, A. Tarancon, S. Barth, O. Casals, R. Jimenez-Diaz, E. Pellicer, J. Rodriguez, J. R. Morante, M. A. Juli, S. Mathur and A. Romano-Rodriguez, *Adv. Funct. Mater.*, 2008, **18**, 2990-2994.
59. M. Epifani, J. D. Prades, E. Comini, E. Pellicer, M. Avella, P. Siciliano, G. Faglia, A. Cirera, R. Scotti, F. Morazzoni and J. R. Morante, *J. Phys. Chem. C*, 2008, **112**, 19540-19546.
60. H. Zeng, G. Duan, Y. Li, S. Yang, X. Xu and W. Cai, *Adv. Funct. Mater.*, 2010, **20**, 561-572.
61. W. Zhou, Y. Liu, Y. Yang and P. Wu, *J. Phys. Chem. C*, 2014, **118**, 6448-6453.

62. Y. Li, J. Zhu, Y. Huang, F. Liu, M. Lv, S. Chen, L. Hu, J. Tang, J. Yao and S. Dai, *RSC Adv.*, 2015, **5**, 28424-28429.
63. X. Li, Q. Yu, C. Yu, Y. Huang, R. Li, J. Wang, F. Guo, Y. Zhang, S. Gao and L. Zhao, *Journal of Materials Chemistry A*, 2015, **3**, 8076-8082.
64. J. Song, E. Zheng, J. Bian, X.-F. Wang, W. Tian, Y. Sanehira and T. Miyasaka, *Journal of Materials Chemistry A*, 2015, **3**, 10837-10844.
65. P. H. Yeh, Z. Li and Z. L. Wang, *Adv. Mater*, 2009, **21**, 4975-4978.
66. S. M. Sze, *Physics of Semiconductor Devices*, 1981.

**Title:** Surface Defects Engineering: Gigantic Enhancement in the Optical and Gas Detection Ability of Metal Oxide Sensor

ToC figure: By using the surface defect engineering, the UV and gas detection abilities can be improved.

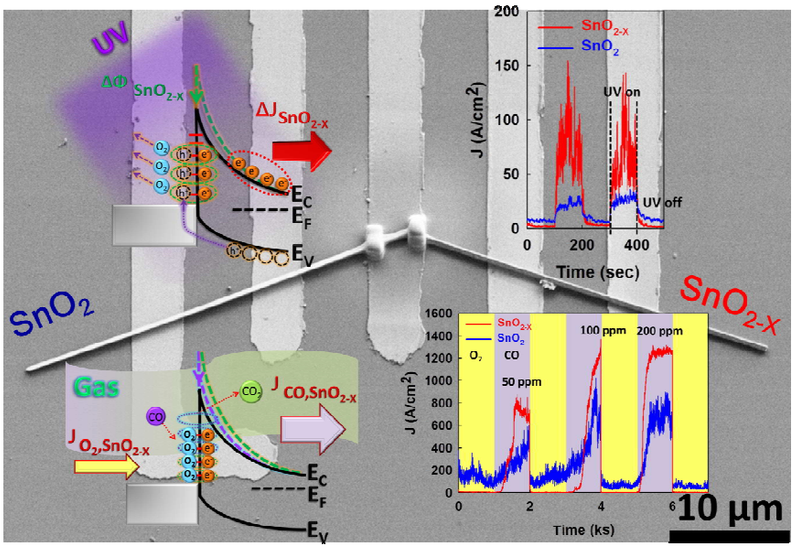

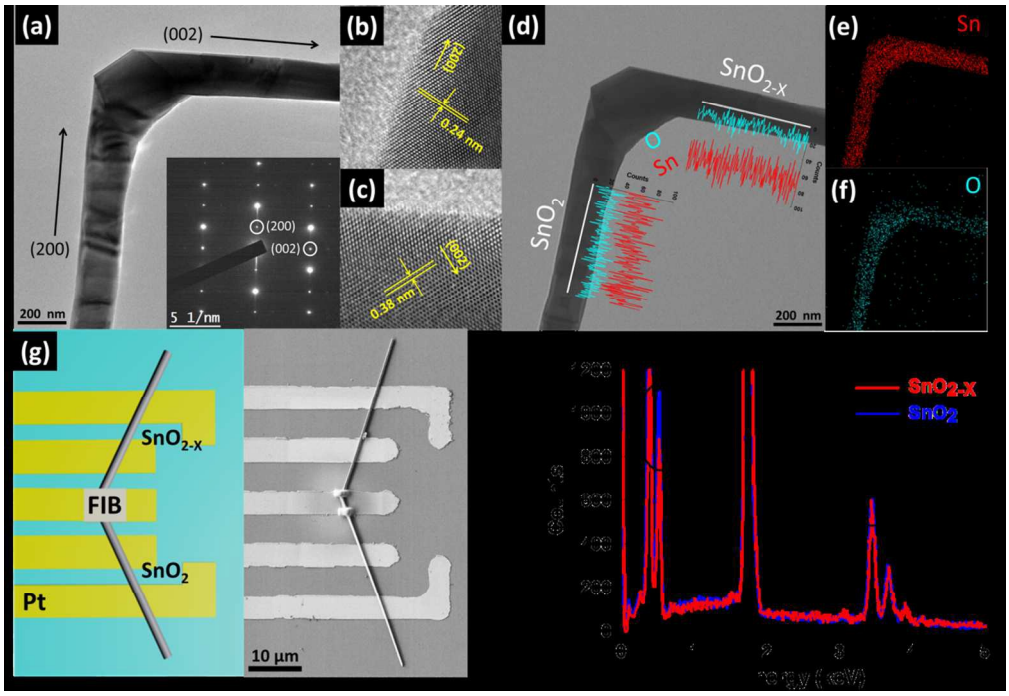


Figure 1. (a) Low magnification TEM image of a kinked SnO2-X/SnO2 nanostructure with the growth orientation changed from (200) to (002), the growth orientation can be indicated by the selected area electron diffraction (SAED) pattern in the inset. (b) and (c) show the high resolution images and lattice constant of SnO2 and SnO2-X, respectively. (d) The Sn and O concentrations of a kinked SnO2-X/SnO2 nanowire can be analyzed by EDS element line scan. (e) and (f) show the elemental mapping of Sn and O, respectively. (g) Schematic diagram and SEM image of SnO2-X/SnO2 nanowire Schottky contacted device. (h) EDS analysis and the atomic percent data of SnO2-X/SnO2 NWs.
149x102mm (220 x 220 DPI)

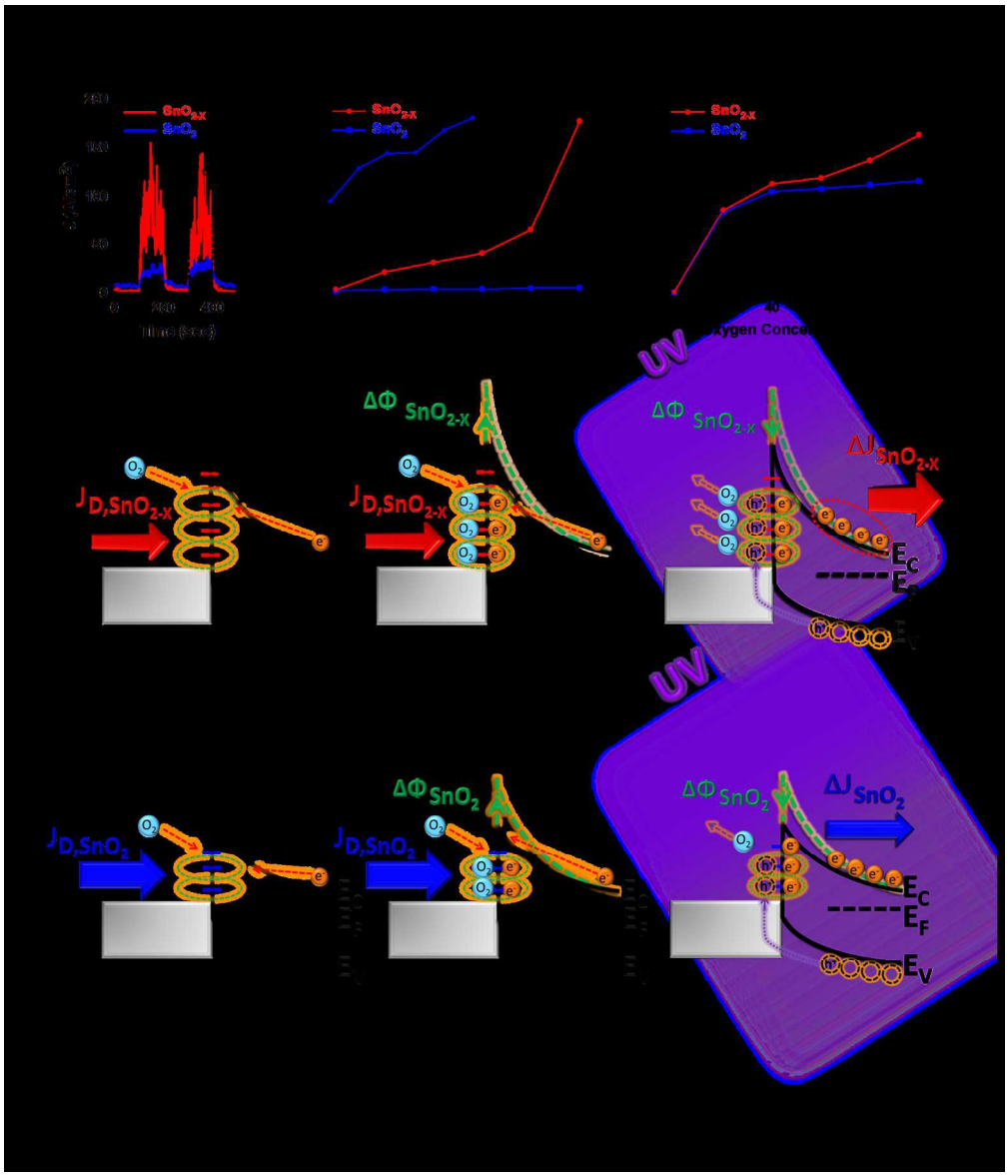


Figure.2 (a) 254nm UV detection performance in 40% oxygen gas environment (with 40% oxygen and 60% nitrogen). (b) The sensitivities in different oxygen concentration of SnO2-X and SnO2 NW devices. (c) and (d) show the mechanism diagrams of SnO2-X and SnO2 NW devices of oxygen molecules interaction at the interface. Step (i) and (ii) represent the adsorption of oxygen molecules. (iii) shows the desorption of oxygen molecules by UV illumined. The SnO2-X NW device has higher sensitivity is because that the VO is higher. When the UV light off, more oxygen molecules were trapped at Schottky contact interface to form O2- and raise the Schottky batrrier height (SBH) to reduce the current, so the Id of SnO2-X NW device was lower. But turn on the UV light, the electron-hole pairs would be generated and O2- would be desorbed by the hole. Because the hole would combine with the O2- to form O2(g) and desorb, that would reduce the SBH to increase the IP. (e) The variation of SBH from vacuum environment to pure oxygen environment (with 100% oxygen) of SnO2-X and SnO2 NW devices.
350x408mm (150 x 150 DPI)

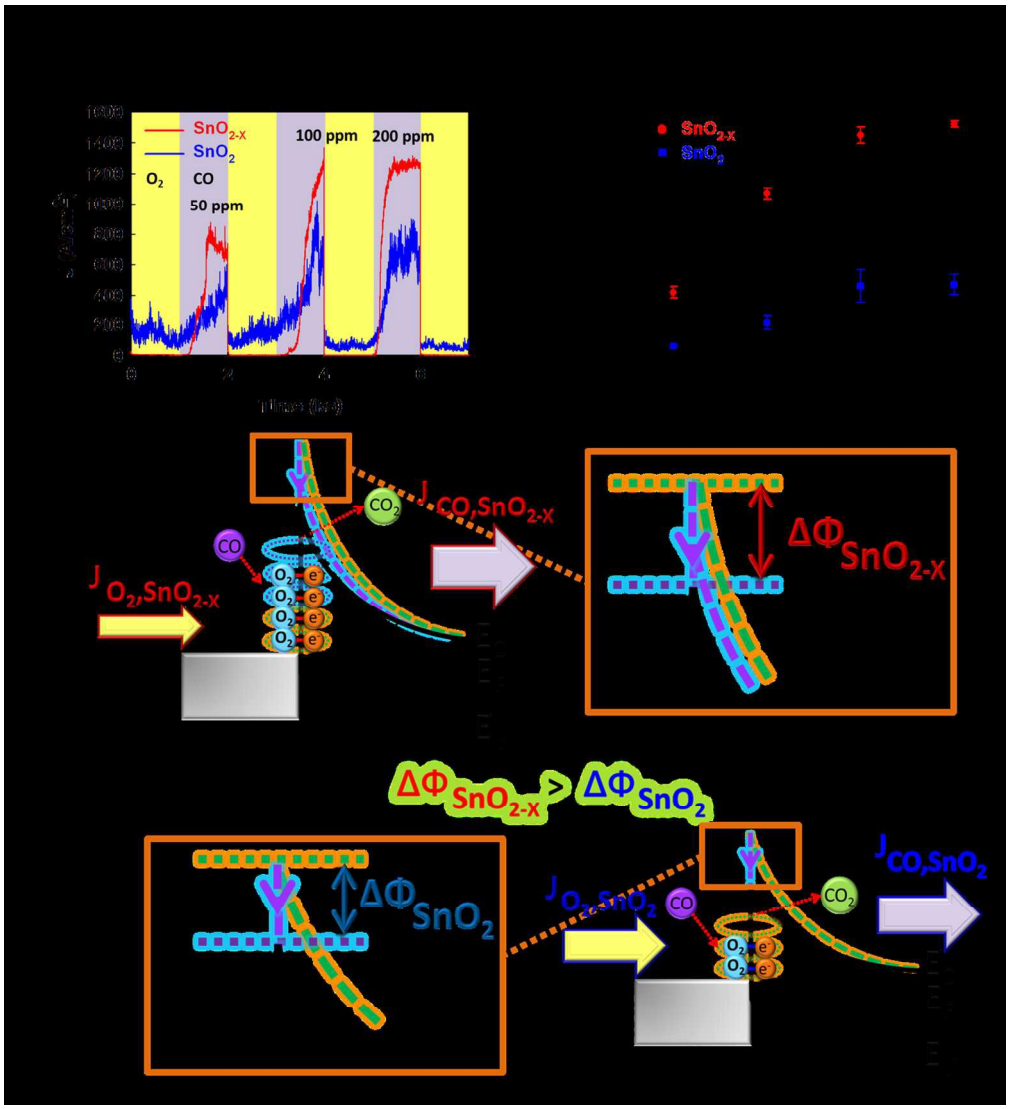


Figure.3 (a) represents detection performance of O2 with different CO concentration sensing at 200 oC operation temperature. (b) The sensitivities of SnO2-X NW device are higher than SnO2 NW device for different CO concentrations detection. (c) shows the detection mechanism of SnO2-X and SnO2 NW devices. Considering CO/O2 alternate-detection, the SBH variation of SnO2-X NW device is larger than SnO2 NW device (△Φ SnO2-X ＞ △Φ SnO2), that is due to the high surface VO density of SnO2-X NW device.
255x280mm (150 x 150 DPI)